UNIVERSITÀ DEGLI STUDI DI BERGAMO
DIPARTIMENTO DI INGEGNERIA DELL'INFORMAZIONE E METODI MATEMATICI°

QUADERNI DEL DIPARTIMENTO

Department of Information Technology and Mathematical Methods

Working Paper

Series "*Mathematics and Statistics*"

n. 5/MS – 2007

Numerical simulation of drug eluting coronary stents: mechanics, fluid dynamics and drug release

by

P. Zunino, C. D'Angelo, L. Petrini, C. Vergara, C. Capelli, F. Migliavacca

° Viale Marconi. 5, I – 24044 Dalmine (BG), ITALY, Tel. +39-035-2052339; Fax. +39-035-562779

[§] L'accesso alle *Series* è approvato dal Comitato di Redazione. I *Working Papers* della Collana dei Quaderni del Dipartimento di Ingegneria dell'Informazione e Metodi Matematici costituiscono un servizio atto a fornire la tempestiva divulgazione dei risultati dell'attività di ricerca, siano essi in forma provvisoria o definitiva.

Numerical simulation of drug eluting coronary stents: mechanics, fluid dynamics and drug release

P. Zunino[♯], C. D'Angelo[♯], L. Petrini[◇], C. Vergara[*], C. Capelli[◇], F. Migliavacca[◇]

December 21, 2007

[♯] Modelling and Scientific Computing (MOX),
Department of Mathematics,
Politecnico di Milano, Italy
[*] Department of Information Technology and Mathematical Methods,
Università degli Studi di Bergamo, Italy
[◇] Laboratory of Biological Structure Mechanics (LaBS),
Department of Structural Engineering,
Politecnico di Milano, Italy

Abstract

Mathematical models and numerical methods have emerged as fundamental tools in the investigation of life sciences. In particular, this is the case of medical devices as cardiovascular drug eluting stents where experimental/clinical evidence may often be very expensive and extremely variable. We present here a complete overview of mathematical models and numerical methods applied to the modelling of drug eluting stents and of their interaction with the coronary arteries. This is a challenging task because it involves mechanics, fluid dynamics and mass transfer processes. In particular, we will focus on the importance of the interplay between all these factors to determine the efficacy of the device.

Keywords: mechanical analysis, blood flow, mass transfer, coupled problems, finite elements, medical devices

1 Introduction

A stent is a small mesh tube that is inserted permanently into a stenotic artery. The stent restores the original value of the arterial section to ensure the physiological

flow rate. One of the problems caused by the stent insertion is the re-narrowing of the treated vessel. To overcome this phenomenon drug-eluting stents (DES) have been recently introduced. Referred to as a *coated* or *medicated* stent, a DES is a normal metal stent that has been coated with a pharmacologic agent (drug) that is known to interfere with the process of restenosis (reblocking). However, the design of such devices is a very complex task because their performance in widening the arterial lumen and preventing further restenosis is influenced by many factors such as the geometrical design of the stent, the mechanical properties of the materials and the chemical properties of the drug that is released. Mathematical models and numerical simulation techniques are appropriate to study such phenomena with the aim to be used as a predictive tool for the effective design of drug eluting stents.

We present in this work a complete review of the mechanics, fluid dynamics and drug release models developed by the authors for the numerical simulation of drug eluting coronary stents. In particular, we will focus on the importance of the interplay between several factors, as the mechanical action exerted by the stent on the wall to determine the final configuration of the artery, as well as the interaction of the blood flow with the drug release process. Indeed, these topics have been already analyzed separately, see [12, 16, 17], but the study of their interaction is still rather new in literature. For example, since the role of the drug is to heal the artery after the implantation of the stent, most of the computational studies on the efficacy of DES have focused their attention on the transport of the drug into the arterial walls, we refer to [15] and references therein for some examples. In most cases, the blood flow is assumed to have a minor influence on the distribution of the drug into the walls. In particular, it is common to consider that the arterial lumen acts as a perfect sink with respect to the drug concentration, because it is rapidly transported away from the location of the stent. Recently, the analysis pursued in [2] suggested that this assumption is not really justified. Indeed, the drug that is apparently lost in the blood stream significantly affects the drug deposition in the portion of the arterial walls downstream to the stent. In this work, we aim to better understand the interaction of the blood flow and the drug deposition into the artery by means of mathematical models and numerical approximation methods, because experimental/clinical evidence for the problem at hand is expensive, extremely variable and provides indirect data that is difficult to correlate with the phenomena we aim to analyze. By consequence, we propose and collect here suitable mathematical models for the stent expansion, the description of hemodynamics and drug release and we focus on their interaction in order to describe the

behavior of realistic drug eluting stents.

The outline of the paper is as follows: in section 2 we introduce the mathematical modelization of the problem at hand, in particular the mechanical stent expansion (section 2.1), the fluid dynamics (section 2.2) and the drug release (section2.3). In section 3 we describe the numerical methods used for the discretization of the proposed problem and in the end in section 4 we present a case study starting fron realistic geometry and data.

2 Mathematical models

The proposed analysis of the stent expansion and the drug elution is made of two consecutive phases. During the former one, a stent is expanded into an atherosclerotic coronary artery. Then, in the latter phase, the configuration of the artery and stent are used for the analysis of the fluid dynamics and drug release.

2.1 Mechanical analysis of the stent expansion into a coronary artery

A previous study [8] showed that the stent expansion modelling techniques influence the output in terms of arterial wall stresses and strains. Hence, for a more reliable description of the deformation induced in an artery by stenting, it is necessary to model the inflation of a polymeric deformable balloon. Nevertheless, the simulation of the stent-balloon expansion in a coronary artery is not a trivial problem: the balloon is typically folded around the catheter and blocked by the crimped stent. Accordingly, the unfolding process requires the solution of a very complex contact problem with large sliding between the surfaces of the balloon itself, the stent struts, the plaque and the inner arterial wall. In this work, we use a simplified model constituted by a balloon, a stent and a coronary artery that are shown in figure 1 (left) in their initial configuration. The analysis is performed in the frame of classical continuum mechanics under the hypothesis of large strain conditions.

In particular for the balloon we consider an initial configuration obtained deflating the full expanded model, developed according to the manufacturer information. In this way, as shown in section 4.1, it is possible to describe the characteristic behavior of a semi-compliant balloon and in particular the strong stiffening at higher pressure, even using an isotropic, linear-elastic material model. Assuming that the elastic strain is small and that the rate of deformation can be regarded as the total strain rate measure, namely $\dot{\varepsilon} = \mathrm{sym}(\mathbf{L})$ where $\mathbf{L}$ is the velocity gradient in the current configuration, the material constitutive model of the implanted baloon,

conveniently written in the incremental form, reads:

$$\dot{\sigma} = \mathbf{D} : \dot{\varepsilon}$$

where $\dot{\sigma}$ is the increment of the Cauchy stress tensor with the elastic tensor $\mathbf{D}$ depending only by the Young's modulus E and the Poisson's ratio ν. Furthermore, also the contribution of the average incremental rigid body rotation of the material has to be taken into account. A different approach may be found in [7].

A realistic geometry is considered for the stent model, which is assumed to be made of 316L stainless steel. The steel is modelled as a homogeneous, isotropic, elasto-plastic material through a Von Mises plasticity model. Assuming again the elastic strain small and the rate of deformation as total strain rate measure, it is possible to describe the inelastic behavior of the stent using the additive strain rate decomposition:

$$\dot{\varepsilon} = \dot{\varepsilon}^{el} + \dot{\varepsilon}^{pl}$$

where $\dot{\varepsilon}^{el}$ and $\dot{\varepsilon}^{pl}$ are the elastic and plastic components of the total strain rate $\dot{\varepsilon}$, respectively. Accordingly with classical plasticity theory, the mathematical description of the stent can be given by the following incremental constitutive equation and associative flow rule:

$$\dot{\sigma} = \mathbf{D} : (\dot{\varepsilon} - \dot{\varepsilon}^{pl}), \quad \dot{\varepsilon}^{pl} = \dot{\lambda} \frac{\partial F(\sigma)}{\partial \sigma}.$$

The limit function is

$$F(\sigma) = \sqrt{\frac{2}{3} J_2'} - K(\alpha) \leq 0,$$

where J_2' is the second invariant of the deviatoric stress tensor $\mathbf{s} = \sigma + p\mathbf{I}$, with $p = -1/3 tr(\sigma)$ the equivalent pressure stress and $\mathbf{I}$ the second order identity tensor and $K(\alpha)$ is the linear isotropic hardening function:

$$K(\alpha) = \sigma_y + K\bar{\varepsilon}^{pl}.$$

The constant σ_y is the yield stress and K is the hardening modulus. The quantity $\bar{\varepsilon}^{pl}$ is the equivalent plastic strain given by:

$$\bar{\varepsilon}^{pl} = \sqrt{\frac{3}{2} \varepsilon^{pl} : \varepsilon^{pl}}.$$

Finally, the consistency parameter $\dot{\lambda}$ has to satisfy the following Kuhn-Tucker com-

plementary conditions:

$$\dot{\lambda} \geq 0;\ F(\sigma) \leq 0;\ \dot{\lambda} F(\sigma) = 0$$

and the consistency requirement $\dot{\lambda}\dot{F}(\sigma) = 0$.

Concerning the arterial wall, we remind that it is a complex structure that consists mainly in three concentric layers: the intima, the media and finally the adventitia. These layers are principally composed of collagene fibers and elastin that give properties of anisotropy and incompressibility. We refer to [10] and the reported references for a more detailed description of the biological aspects and of the advanced computational models available in literature.

In our simplified model, the coronary artery is described as a hollow cylinder partitioned into three layers of equal thickness, representing the intima, the media and the adventitia. A bond of perfect adhesion exists between each pair of vessel layers. For describing the mechanical behavior of each layer, we use a hyperelastic isotropic constitutive model based on a reduced polynomial strain energy density function U, of sixth order:

$$\begin{aligned} U = C_{10}(\bar{I}_1 - 3) + C_{20}(\bar{I}_1 - 3)^2 + C_{30}(\bar{I}_1 - 3)^3 \\ + C_{40}(\bar{I}_1 - 3)^4 + C_{50}(\bar{I}_1 - 3)^5 + C_{60}(\bar{I}_1 - 3)^6, \quad (1) \end{aligned}$$

where $\bar{I}_1$ is the first invariant of the Cauchy-Green tensor

$$\bar{I}_1 = \bar{\lambda}_1^2 + \bar{\lambda}_2^2 + \bar{\lambda}_3^2, \quad \text{with } \bar{\lambda}_i = J^{-1/3}\lambda_i,$$

where $\bar{\lambda}_i$ are the principal stretches and J is the total volume ratio.

The model is not able to take into account residual stresses present in the load-free artery configuration and the overstretch of the non-diseased part of the lesion due to supraphysiological loading induced by balloon expansion: we refer to [7] for a deeply discussion of these aspects. Moreover, in our work the plaque is not considered. This choice was motivated by the observation that the lack of experimental data about the material properties as well as the poor knowledge of the atherosclerotic plaque growing process make totally arbitrary any modelling choice. It is clear that the availability of more information about the mechanical behavior and the use of more refined models of atherosclerotic tissue could give more precise information about the effects of the stenting process. However, we believe that even the simplified model herein introduced does not play down our

methodology.

To reduce the computational time we study the expansion of only a single stent unit, i.e. a closed axial stent segment. A previous analysis [8] showed that this choice is sufficient to represent the mechanical behavior of the stent. Accordingly, we perform the analysis on a portion of the coronary artery whose length is sufficient to avoid boundary effects. The dimension of the balloon is coherently set, conserving the stent/balloon length ratio usually adopted in the practice.

As regards the boundary conditions of the model, the outer cross sections of the artery indicated with $\Gamma_{n,w}$ in figure 1 (left) are constrained in the longitudinal direction to simulate the fact that the considered model is not a stand-alone segment but is part of a whole coronary artery. Furthermore, in a axial section located in the center of the artery, three nodes forming the vertexes of an equilateral triangle are constrained in the tangential direction to avoid the rotation of the structure. These conditions allow the radial expansion of the artery. As regards the stent, we apply boundary conditions which constrain in the longitudinal and tangential directions three nodes forming the vertexes of an equilateral triangle in the medial cross section of the stent itself, indicated with $\Gamma_{n,sc}$ in figure 2. To avoid potential rigid displacements in the balloon, three nodes forming an equilateral triangle are constrained in axial and circumferential directions in the central cross section, indicated with $\Gamma_{n,bc}$ in figure 2. In addition, the radial and tangential displacements of the two nodes located on the heads of the balloon are restricted to mimic the bond to the catheter. The expansion of the device is simulated imposing a pressure on the internal surface of the deflated balloon. Denoted with Γ the internal surface of the artery, with Γ_s the surface of the stent and with Γ_b the surface of the balloon, see figure 1 (left), during the analysis the interaction between these parts is taken into account introducing a frictionless contact.

2.2 Fluid dynamics models in the lumen and in the arterial walls

Thanks to the assumption that coronary arteries treated with cardiovascular stents are large enough to apply a Newtonian model for blood rheology, we consider the Navier-Stokes equations for the fluid dynamics in the arterial lumen. We denote with Ω_f a portion of a coronary artery where we set up our analysis. This is the cylindric channel deformed by the introduction and the expansion of a stent, as described in the previous sections. We denote with Γ_{in} and Γ_{out} the proximal and distal sections since they coincide with the inflow and outflow sections of the domain Ω_f. The remaining part of the boundary of Ω_f can be subdivided in two parts,

the interface with the arterial wall and the stent. The former is denoted with Γ and the latter with $\Gamma_{s,f}$. In conclusion we obtain $\partial\Omega_f = \Gamma_{in} \cup \Gamma_{out} \cup \Gamma_{s,f} \cup \Gamma$, as shown in figure 1 (right). Finally, we denote with $\mathbf{n}_f$ the outward unit normal vector on $\partial\Omega_f$.

To analyze the drug release process on a significant time scale we need to consider a time period containing several thousands of heartbeats. This is a challenging difficulty for the drug release model, which is common to all ordinary/partial differential equations with highly oscillating coefficients or forcing terms. To override this difficulty at a preliminary level, we consider the mean value of the pulsatile blood flow and simultaneously we assume that the arterial walls are rigid. Then, the blood flow is provided by the steady Navier-Stokes equations,

$$-\mu\Delta\mathbf{v}_f + (\mathbf{v}_f \cdot \nabla)\mathbf{v}_f + \nabla p_f = \mathbf{0} \quad \text{and} \quad \nabla \cdot \mathbf{v}_f = 0, \quad \text{in } \Omega_f, \tag{2}$$

where $\mathbf{v}_f$ is the blood flow velocity, p_f the corresponding pressure and μ the blood dynamic viscosity. Equation (2) is complemented by suitable boundary conditions specifying a parabolic inflow profile, $\mathbf{v}_f = \mathbf{v}_{in}$ on Γ_{in}, perfect contact between the blood, the arterial walls and the stent, $\mathbf{v}_f = 0$ on $\Gamma \cup \Gamma_w$, and zero traction force at the outflow, $p\mathbf{n}_f - \mu\nabla\mathbf{v}_f\mathbf{n}_f = 0$ on Γ_{out}.

We remind that the flow is not restricted to the arterial lumen. Indeed, blood plasma filtrates with a velocity $\mathbf{v}_w$ from the inner to the outer part of the arterial walls under the action of blood pressure. As observed in [23, 13, 17] this phenomenon is extremely important for the transfer of large molecules (as for instance low density lipoproteins) from the blood flow to the arterial walls, because the diffusivity of such molecules is extremely low. For smaller molecules, such as oxygen but also some of the drugs that are released from stents, the mass transfer form the lumen to the arterial walls is diffusion dominated rather than governed by advection. This is shown in [23] by means of dimensional analysis. For this reason, in this study we neglect the advective phenomena into the arterial walls ($\mathbf{v}_w = \mathbf{0}$) and we refer to [13, 17] for a detailed description of the corresponding models.

2.3 A mathematical model for drug release

We assume that the drug released by the stent behaves as a passive scalar. This statement holds true under the assumption that the drug does not react with the arterial walls. This is a zero-level simplification of a number of chemical phenomena that involve the drug as a ligand and suitable sites of the extracellular matrix as

receptors. It is well known that such phenomena may strongly influence the distribution of the drug into the arterial walls, as discussed in [22, 24]. However, it is not definitely clarified how to translate these phenomena into equations and how to feed them with parameters. By consequence, our drug release model features just one chemical specie, the drug, that is governed by standard advection-diffusion equations. Furthermore, the drug we will consider in the numerical experiments is heparin, a relatively small molecule with non negligible diffusive properties. Then, for the interaction of the mass transfer in the lumen and in the arterial walls we address the model described and analyzed in [19] for the transport of oxygen. As already mentioned, in this case the advective phenomena into the arterial walls are neglected. Concerning the coronary artery, we make here a simplification of the complex multilayered structure of the wall, more precisely we assume that the arterial wall is an homogeneous medium, whose physical properties are, for simplicity, the ones corresponding to the intermediate layer, namely the *media*. This assumption can be easily removed at the computational level because the deformed configuration of the three layers of the artery is provided by the mechanical analysis described in section 2.1. However, this improvement becomes troublesome in practice, because of the lack of reliable data on the transport properties of each layer with respect to the drug. To our knowledge, only average values for the complete arterial wall are available, we refer to [14] for the case of heparin. In this setting, let Ω_w be the truncated portion of the arterial walls corresponding to Ω_f. We denote with Γ_a the interface of the arterial wall with the outer tissue, with $\Gamma_{n,w}$ the artificial sections originated by the truncation of the artery and with $\Gamma_{s,w}$ the interface of the stent with the arterial wall. Moreover, let $\mathbf{n}_w$ be the outward unit normal vector relative to Ω_w. Furthermore, contrarily to the assumptions adopted for the fluid dynamics, we consider the time dependent case, because the drug release process is intrinsically transient and it dies out in a long but finite time. Then, the governing equation for the drug concentration read as follows,

$$\partial_t c_* + \nabla \cdot (-D_* \nabla c_* + \mathbf{v}_* c_*) = 0 \text{ in } \Omega_*, \text{ with } * = f, w, \tag{3}$$

together with a condition prescribing the initial state of the concentration in the blood stream and into the arterial walls, $c_*(t=0) = 0$ in Ω_* and suitable boundary conditions. For the arterial lumen, Ω_f, on the inflow boundary we prescribe $c_f = 0$ on Γ_{in} since the blood does not contain drug proximally to the stent. Assuming that the outflow boundary is far enough to the stent, we can neglect any diffusive

effects across this section and set $\nabla c_f \cdot \mathbf{n}_f = 0$ on Γ_{out}. Also for the arterial wall we prescribe $\nabla c_w \cdot \mathbf{n}_f = 0$ on $\Gamma_a \cup \Gamma_{n,w}$. According to [19], for the transmission conditions between Ω_f and Ω_w we take into account the endothelium, a single layer of cells impermeable to the blood flow. The endothelium is modelled as a membrane at the interface between the lumen and the arterial walls, corresponding to Γ, having a permeability P with respect to the transfer of drug. This model allows to take into account the possible shear-dependent behavior of mass flux through the endothelium. This is an interesting problem that has been addressed in [20] and [21] for oxygen and albumin transport respectively. A similar discussion can be also addressed for the diffusion parameter in the blood flow, namely D_f. Indeed, according to [26] the rotation of red blood cells due to flow vorticity may lead to augmented transport properties. However, the intrinsic difficulty of this studies is to quantify the dependence of the endothelial permeability and blood diffusivity with respect to the fluid dynamics quantities as shear stresses or shear rates. Since to our knowledge there are no available data on this dependence in the case of drugs, we do not include this feature in our model and we assume that the permeability P and the diffusivity D_f are constant and uniform. Then, the coupling between equations (3) is provided by the following conditions,

$$-D_f \nabla c_f \cdot \mathbf{n}_f = -D_w \nabla c_w \cdot \mathbf{n}_f \quad \text{and} \quad -D_w \nabla c_w \cdot \mathbf{n}_w = P(c_w - c_f), \quad \text{on } \Gamma.$$

We observe that these conditions can be rewritten as follows,

$$-D_f \nabla c_f \cdot \mathbf{n}_f = P(c_f - c_w) \quad \text{and} \quad -D_w \nabla c_w \cdot \mathbf{n}_w = P(c_w - c_f) \quad \text{on } \Gamma. \tag{4}$$

The latter formulation has the advantage to be symmetric with respect to the lumen and the arterial walls. As shown in [19] this represents an advantage both for the analyis and the numerical approximation of the coupled problem.

Finally, particular attention should be dedicated to the condition on the interface between the stent and the lumen, because it is primarily responsible to determine the drug release rate. We remind that DES for cardiovascular applications are miniaturized metal structures that are coated with a micro-film containing the drug that will be locally released into the arterial walls for healing purposes. The thickness of this film generally lays within the range of microns. Owing to the fact that the stent coating is extremely thin, we apply the model proposed in [25] where

it has been derived the following formula for the release rate,

$$J(t,\mathbf{x}) = \varphi(t)(c_s^0 - c_*) \text{ on } \Gamma_{s,*} \text{ with } * = f, w, \quad t > 0, \text{ for any } \mathbf{x} \in \Gamma, \tag{5}$$

being c_s^0 the initial drug charge of the stent that is equal to the unity in the undimensional setting for the concentration. Given the thickness of the stent coating, Δl, and its diffusion parameter, D_s, the scaling function $\varphi(t)$ is defined as follows,

$$\varphi(t) = \frac{2D_s}{\Delta l} \sum_{n=0}^{\infty} e^{-(n+1/2)^2 kt} \quad \text{with} \quad k = \pi^2 D_s / \Delta l^2. \tag{6}$$

The derivation of (5) is similar to the procedure that leads to the well known Higuchi formula [9], that provides the drug concentration c_s into a semi-indefinite planar slab (with axial coordinate z) representing the stent coating, under the assumption that the external medium acts as a prefect sink,

$$\frac{c_s(t,z)}{c_s^0} = 1 - \text{erf}\left(\frac{z}{\sqrt{4D_s t}}\right), \quad z \in (-\infty, 0), \; t > 0, \text{ for any } \mathbf{x} \in \Gamma. \tag{7}$$

However, equation (6) has the advantage to avoid the restrictive assumptions of Higuchi formula (7). Owing to (5), the boundary condition on $\Gamma_{s,f}$ and $\Gamma_{s,w}$ for equation (3) turns out to be the following Robin type condition,

$$-D_* \nabla c_* \cdot \mathbf{n}_* + \varphi(t)(c_s^0 - c_*) = 0 \text{ on } \Gamma_{s,*} \text{ with } * = f, w.$$

The initial/boundary value problems relative to equations (2) and (3) are now ready to be approximated by means of suitable numerical methods.

3 Numerical methods

3.1 Numerical simulation of the stent expansion

The strong nonlinearity of the problem, due to material and contact constraints, suggested the use of an explicit dynamics analysis procedure for its solution in the frame of the finite element method. In particular, the commercial code ABAQUS/ Explicit v. 6.4 is employed. The space dependence of the mechanical model is discretized with eight-node iso-parametric brick elements with reduced integration for the stent and the artery, while we adopt four-nodes or three-nodes membrane elements with reduced integration to discretize the balloon.

The treatment of the dynamic problem is based upon the implementation of an explicit integration rule together with the use of lumped element mass matrices. In particular the explicit central difference integration rule is used for integrating the motion equation. Let $\mathbf{u} \in \mathbb{R}^3$ be the displacement of each element node.

The known values of the acceleration $\ddot{\mathbf{u}}$ from previous increment (n), of the velocity $\dot{\mathbf{u}}$ from previous mid-increment $(n+1/2)$, as well as of the time increment Δt at the current $(n+1)$ and the previous (n) increment, are used for calculating velocity and displacement at the current interval:

$$\dot{\mathbf{u}}^{n+\frac{1}{2}} = \dot{\mathbf{u}}^{n-\frac{1}{2}} + \frac{\Delta t^{n+1} + \Delta t^n}{2} \ddot{\mathbf{u}}^n,$$
$$\mathbf{u}^{n+1} = \mathbf{u}^n + \Delta t^{n+1} \dot{\mathbf{u}}^{n+\frac{1}{2}}.$$

If diagonal element mass matrices $\mathbf{M}$ are used, it is straightforward to calculate the acceleration at the beginning of the increment simply inverting the dynamic equilibrium equation:

$$\ddot{\mathbf{u}}^n = \mathbf{M}^{-1}(\mathbf{F}^n - \mathbf{P}^n),$$

with $\mathbf{F}^n$ and $\mathbf{P}^n$ the external applied forces and the internal element forces, respectively. Peculiar attention has to be paid to the initial condition. The central difference operator is conditionally stable, and the stable time increment Δt has to satisfy the relation:

$$\Delta t \leq \frac{2}{\omega_{max}},$$

where ω_{max} is the highest eigenvalue in the system. If small amount of damping is introduced to control high frequency oscillations, the time increments have to satisfy:

$$\Delta t \leq \frac{2}{\omega_{max}}(\sqrt{1+\xi^2} - \xi),$$

with ξ the fraction of critical damping in the highest mode.

Since the aim of the analysis is to define a stented artery configuration in the steady state condition,a quasi-static analysis is performed. Hence, we increase the density of the materials, we smooth the application of loading and set the time step of the simulations to 1 s, in order to model the process in the shortest time period in which inertial forces remain insignificant. This hypothesis is verified evaluating that the ratio between kinetic and internal energies of the model does not exceed the value 5%, as suggested by the ABAQUS manual.

To take into account the contact between different parts, we use the contact

pair algorithm proposed in ABAQUS/Explicit, see ABAQUS version 6.5 Online Documentation, and we adopt a kinematic predictor/corrector contact algorithm to strictly enforce contact constraints (no penetrations are allowed), coupled with a finite sliding approach to account for the relative motion of the two surfaces forming the contact pair, and an exponential pressure-overclosure relationships to specify the interaction behavior.

3.2 Numerical simulation of the fluid dynamics and of the drug release

As already seen, our drug release model involves the coupling of the blood flow equations with an advection-diffusion problem, namely equations (2) and (3). In these models, the advection-diffusion equations depend on the fluid dynamics through the advective field. Hence the fluid dynamics problem is solved at a first step, and then we solve the mass transfer problem.

For the space discretization of the space-dependent partial differential operators, we apply the finite element method. In particular, for what concerns the Navier–Stokes equations we have adopted a linear approximation based on $\mathbb{P}^1 - \mathbb{P}^1$ elements that have been stabilized with respect to pressure/velocity coupling and to a high local Reynolds number by means of the interior penalty scheme proposed in [3]. Furthermore, we have adopted the classical Picard's scheme for the treatment of the nonlinear term.

Concerning the advection-diffusion equations we apply $\mathbb{P}^1$ elements for the space discretization and implicit Euler scheme for the approximation of the time dependence. We observe that equation (3) is advection dominated in Ω_f. As it is well known, finite element techniques could be inaccurate when facing such problems and resorting to a stabilization technique becomes mandatory. Different strategies can be pursued in this regard, we apply again interior penalty schemes, developed in [4] for advection-diffusion-reaction problems and also applied to coupled problems in [5].

A further difficulty is related to the fact that we consider phenomena that take place both into the blood flow and into the arterial tissues. In particular, the coupled problem given by equations (3) and by the matching conditions (4) can not be reformulated as a problem governed by a unique differential operator on a single domain. For this reason, we focus our attention on suitable iterative methods in order to split (3)-(4) into a sequence of independent problems. To this purpose, a general theory is discussed for instance in [18], for the case of linear symmetric

problems. However, the presence of a non negligible advection term makes our case to be governed by a strongly unsymmetric operator into Ω_f. For this reasons, we refer to [19] where a case equivalent to (3)-(4) is analyzed. The main features of this approach are reported in the following section.

All the aforementioned schemes are implemented into a the finite element library *LIFE V*, developed at MOX - Politecnico di Milano, INRIA - Paris and CMCS - EPFL - Lausanne, see www.lifev.org .

3.2.1 An iterative splitting algorithm for the coupled problem of drug release

To address in detail the iterative splitting method for the drug release problem, we refer to the time-discrete setting. To this purpose, we subdivide the time interval $[0,T]$ in N time steps t^n and $n = 1,\dots,N$, where $\Delta t^n = t^{n+1} - t^n > 0$ is possibly non uniform, and use backward Euler finite difference schemes. Since all the relevant equations deal only with unknowns evaluated at the time step t^n, for notational convenience we drop the index n. The time index will be explicitly indicated only when referring to a time step different than t^n. Then, problem (3)-(4) complemented with boundary and initial conditions can be reformulated as follows: for any time step t^n, find a sequence c_f^k, c_w^k such that,

$$\begin{cases} \frac{1}{\Delta t}c_f^k + \nabla\cdot(-D_f\nabla c_f^k + \mathbf{v}_f c_f^k) = \frac{1}{\Delta t}c_f^{n-1} & \text{in } \Omega_f, \\ c_f^k = 0, & \text{on } \Gamma_{in}, \\ \nabla\cdot c_f^k\cdot\mathbf{n}_f = 0 & \text{on } \Gamma_{out}, \\ -D_f\nabla c_f^k\cdot\mathbf{n}_f + \varphi(t^n)(c_s - c_f^k) = 0 & \text{on } \Gamma_{s,f}, \\ -D_f\nabla c_f^k\cdot\mathbf{n}_f = P(c_f^k - c_w^{k-1}), & \text{on } \Gamma, \end{cases} \tag{8}$$

$$\begin{cases} \frac{1}{\Delta t}c_w^k + \nabla\cdot(-D_w\nabla c_w^k) = \frac{1}{\Delta t}c_w^{n-1} & \text{in } \Omega_w, \\ \nabla c_w^k\cdot\mathbf{n}_w = 0 & \text{on } \Gamma_{n,w}\cup\Gamma_a, \\ -D_w\nabla c_w^k\cdot\mathbf{n}_w + \varphi(t^n)(c_s - c_w^k) = 0 & \text{on } \Gamma_{s,w}, \\ -D_w\nabla c_w^k\cdot\mathbf{n}_w = P(c_w^k - c_f^k), & \text{on } \Gamma. \end{cases} \tag{9}$$

Equations (8) and (9) can be reformulated weakly. It consists of linear second-order problems whose well-posedness in the classical Sobolev spaces $H^1(\Omega_f)$, $H^1(\Omega_w)$ can be easily proven by means of the Lax-Milgram lemma, which also ensures the existence and uniqueness of solutions at the discrete level. The well posedness at the discrete level is maintained also when the Galerkin approximation of problem (8) is stabilized by means of the interior penalty scheme. We refer to [4] for a complete analysis of this method. Finally, it is possible to prove the convergence of the sequence $c_f^k,\ c_w^k$ to the solution of the coupled problem, denoted with $c_f,\ c_w$. We remind the main result in the following proposition.

Proposition 1 (Convergence of the iterative splitting method) *The iterative method defined by equations* (8) *and* (9) *is convergent. Let $e_*^k = c_* - c_*^k$ be the iterative splitting error with $* = f, w$, where c_* is the solution of the coupled problem* (3)-(4) *and c_*^k is the sequence generated by* (8) *and* (9)*. More precisely we have:*

$$\lim_{k\to\infty} \|c_* - c_*^k\|_{H^1(\Omega_*)} = 0 \text{ with } * = f, w.$$

A similar result holds true at the discrete level for both the Galerkin and the interior penalty stabilized discretizations. The convergence rate may depend on the physical data but not on the mesh size h.

Proof. By subtracting (8)-(9) from the equations of the coupled problem, namely (3)-(4), we obtain the governing equations from the splitting error e_*^k. Their weak formulation reads as follows,

$$\begin{aligned} a_f(e_f^k, v_f) + \int_\Gamma P e_f^k v_f &= \int_\Gamma P e_w^{k-1} v_f,\ \forall v_f \in H^1(\Omega_f), \\ a_w(e_w^k, v_w) + \int_\Gamma P e_w^k v_w &= \int_\Gamma P e_f^k v_w,\ \forall v_w \in H^1(\Omega_w), \end{aligned}$$

being $a_f(\cdot,\cdot)$ and $a_w(\cdot,\cdot)$ the bilinear forms associated to problems (8) and (9) without the contributions of the coupling terms, which have been explicitly reported. It is easily seen that these bilinear forms are coercive with respect to the standard H^1-norm on Ω_* with suitable constants α_* that may depend on the diffusivity parameter D_*. Choosing $v_* = e_*^k, * = f, w$ and exploiting the coercivity and the Cauchy-Schwarz inequality we obtain,

$$\begin{aligned} \alpha_f \|e_f^k\|^2_{H^1(\Omega_f)} + \|P^{\frac{1}{2}} e_f^k\|^2_{L^2(\Gamma)} &\le \|P^{\frac{1}{2}} e_f^k\|_{L^2(\Gamma)} \|P^{\frac{1}{2}} e_w^{k-1}\|_{L^2(\Gamma)}, \\ \alpha_w \|e_w^k\|^2_{H^1(\Omega_w)} + \|P^{\frac{1}{2}} e_w^k\|^2_{L^2(\Gamma)} &\le \|P^{\frac{1}{2}} e_f^k\|_{L^2(\Gamma)} \|P^{\frac{1}{2}} e_w^k\|_{L^2(\Gamma)}. \end{aligned}$$

Owing to the trace theorem there exists a constant C_* such that $\|v\|^2_{L^2(\Gamma)} \leq C_* \|v_*\|^2_{H^1(\Omega_*)}$. The application of this inequality into the equations above, together with the simplifying assumption that P is a constant parameter, leads to the following results,

$$\left(1+\frac{\alpha_f}{C_* P}\right)\|P^{\frac{1}{2}} e_f^k\|_{L^2(\Gamma)} \leq \|P^{\frac{1}{2}} e_w^{k-1}\|_{L^2(\Gamma)}, \quad \left(1+\frac{\alpha_w}{C_* P}\right)\|P^{\frac{1}{2}} e_w^k\|_{L^2(\Gamma)} \leq \|P^{\frac{1}{2}} e_f^k\|_{L^2(\Gamma)},$$

that can be combined in order to obtain,

$$\|P^{\frac{1}{2}} e_f^k\|_{L^2(\Gamma)} \leq \left(1+\frac{\alpha_f}{C_* P}\right)^{-1}\left(1+\frac{\alpha_w}{C_* P}\right)^{-1}\|P^{\frac{1}{2}} e_f^{k-1}\|_{L^2(\Gamma)}.$$

Together with the trace inequality, this proves the desired result.

Finally, we observe that the proof can be immediately extended to the case of the Galerkin discretization method. Since the constants that determine the error reduction factor in the final inequality do not depend on the discretization method, we conclude that the convergence rate is always independent on the discretization parameter h. We also observe that the introduction of the interior penalty stabilization term in the discrete equation for c_f does not prevent the convergence of the iterations. Indeed, the proof remains unchanged if we replace to $a_f(\cdot,\cdot)$ the following stabilized bilinear form,

$$\hat{a}_f(c_f, v_f) = a_f(c_f, v_f) + J_f(c_f, v_f), \quad \text{with}$$
$$J_f(c_f, v_f) = \sum_{e \in F_h^i} \gamma_{ip} h_e^2 \|\mathbf{v}_f \cdot \mathbf{n}_e\|_{L^\infty(e)} \int_e [\nabla c_f \cdot \mathbf{n}_e][\nabla v_f \cdot \mathbf{n}_e],$$

being F_h^i the collection of all the internal edges ($d=2$) or faces ($d=3$) e of the computational mesh on $\Omega_f \subset \mathbb{R}^d$, whose normal vector and $(d-1)$-dimensional measure are denoted with $\mathbf{n}_e$ and h_e respectively. $\square$

Remark 1 (Robustness with respect to singularly perturbed problems) We observe that the proof of proposition 1 suggests that the iterative method may not converge in the case of singularly perturbed problems, namely when $D_* \to 0$. In this case the coercivity constants vanish and correspondingly the estimate of the error reduction constant at each iteration approaches the unity. This is not an intrinsic problem of the iterative method. In fact, the proof can be easily adapted to the case of singularly perturbed problems by virtue of the introduction of the energy norm,

$$|||v_*|||^2 = \|D_*^{\frac{1}{2}} v_*\|^2_{H^1(\Omega_*)} + \|(\Delta t)^{-\frac{1}{2}} v_*\|^2_{L^2(\Omega_*)}.$$

We notice that the bilinear forms $a_*(\cdot,\cdot)$ are coercive with respect to this norm, uniformly with respect to the diffusivity parameter D_*, namely $a_*(v,v) \geq |||v_*|||^2$ for any $v \in H^1(\Omega_*)$. The proof of proposition 1 can be straightforwardly adapted to this case. Indeed, starting from the splitting error equations we easily obtain that,

$$|||e_f^k|||^2 + \|P^{\frac{1}{2}} e_f^k\|^2_{L^2(\Gamma)} \leq \frac{1}{2}\|P^{\frac{1}{2}} e_f^k\|_{L^2(\Gamma)} + \frac{1}{2}\|P^{\frac{1}{2}} e_w^{k-1}\|_{L^2(\Gamma)},$$
$$|||e_w^k|||^2 + \|P^{\frac{1}{2}} e_w^k\|^2_{L^2(\Gamma)} \leq \frac{1}{2}\|P^{\frac{1}{2}} e_f^k\|_{L^2(\Gamma)} + \frac{1}{2}\|P^{\frac{1}{2}} e_w^k\|_{L^2(\Gamma)}.$$

Combining these inequalities and summing up from $k = 1$ to $k = M$ we get,

$$\sum_{k=1}^{M} \left(|||e_f^k|||^2 + |||e_w^k|||^2 \right) + \frac{1}{2}\|P^{\frac{1}{2}} e_w^M\|^2_{L^2(\Gamma)} \leq \frac{1}{2}\|P^{\frac{1}{2}} e_w^0\|^2_{L^2(\Gamma)}.$$

The convergence of the sequences c_f^k and c_w^k is obtained passing to the limit for $M \to \infty$. However, in this case the convergence rate of the iterations can not be explicitly characterized.

3.2.2 A-priori adapted time stepping

The drug release form the stent is a transient process that features a very fast initial phase that progressively slows down until almost all the drug has been delivered. The dynamics of the release rate with respect to time can be approximated by means of the Higuchi formula, namely equation (7), which provides an explicit estimate for the flux of drug outgoing the stent,

$$J_{hig}(t,\mathbf{x}) = \sqrt{\frac{D_s c_s^2}{\pi t}},\ t \in (0,T],\ \mathbf{x} \in \Gamma.$$

This formula, which is exact for the limit case $t \to 0$ but inaccurate for long time periods, provides an effective way to adapt the time advancing step to the transient release process, as discussed in [25]. For simplicity, we set up an adaptivity strategy based on the increment of the amount of drug that is released from the stent to the arterial walls. More precisely, we aim to find a suitable sequence of time steps, t^n, such that a constant fraction of the total amount of drug is released in each time slab. We notice that this problem can be solved exactly in the framework of the Higuchi model. In particular, let η be the constant fraction of drug that we aim to release at each time step. Let us introduce a uniform partition of $[0,1]$ into sub-intervals of length η, such that $N := 1/\eta$ is an integer, for simplicity. Cor-

respondingly, we define the sequence $f^n = n\eta$ with $n = 0,\ldots,N$. The time steps that we look for, correspond to the mapping of the sequence f^n into the interval $[0, t_e := (\pi\Delta l^2)/(4D_s)]$ by means of the incremental version of equation (7),

$$t^n = \frac{\pi\Delta l^2}{4D_s}(f^n)^2, \quad n = 0,\ldots,N,$$
$$\Delta t^n = \frac{\pi\Delta l^2}{4D_s}\left[(f^n)^2 - (f^{n-1})^2\right] = \frac{\pi\Delta l^2}{4D_s}\eta^2(2n-1), \quad n = 1,\ldots,N.$$

We notice that Δt^n grows linearly with respect to η. After N steps, this scheme reaches the time t_e where all the drug should have been delivered, according to the inexact Higuchi model. Then the time step can be maintained constant and equal to Δt^N. For a time interval of 1 day, the numerical experiments presented in [25] show that this a-priori adapted time stepping ensures that the amount of drug delivered in each time slab is almost constant also in the case of the release model (6) applied in our case. Reminding that our time discretization scheme is only first order accurate, the key point is to choose a suitably small increment, η, that ensures an effective compromise between computational efforts and accuracy, in particular mass conservation.

4 A case study: influence of the arterial stent positioning on blood flow and the drug release

We aim to study the interaction of the blood flow with the drug released from the stent. This task is particularly challenging because the complex geometry of the stent highly perturbs the local flow and this significantly influences the path of the drug released into the lumen. We split this analysis in three parts. First of all we focus on the structural mechanics generated by the stent expansion; secondly we analyzed the fluid dynamics, trying to put into evidence the main features of the flow around the stent. Lastly, we study how this flow influences the drug release.

4.1 Analysis of the stent expansion

The stent used in this study resembles the coronary Cordis BX-Velocity (Johnson & Johnson, Interventional System, Warren, NJ, USA). The stent geometry, see figure 2 (left), is created using Rhinoceros 3.0 Evaluation CAD program (McNeel & Associates, Indianapolis, IN, USA), after an acquisition of the Cordis dimensions by

the use of a Nikon SMZ800 stereo microscope (Nikon Corporation, Tokyo, Japan). The length of the unit of the stent considered in the analysis is 3.62 mm, the inner radius 0.6 mm and the thickness 0.14 mm. A mesh of 14951 8-node cubic element is generated. For the material parameters we refer to [1] where the Young's modulus is E=193 GPa, the Poisson's coefficient ν=0.3 and the yield stress σ_y= 205 MPa; we take into account the degradation of the hardening modulus, varying from K=1500 MPa and K=97 MPa, using the ABAQUS option of defining a a linear piecewise isotropic hardening.

The balloon is designed with a radius of 1.5 mm and length of 8 mm. The mesh consists of 11650 4-nodes membrane elements and 220 3-nodes membrane elements (thickness = 0.05 mm) in order to obtain the balloon heads. The characteristic parameters of the material are the Young's modulus E=900 GPa and the Poisson's coefficient ν=0.3. To obtain the initial deflated configuration of the balloon, a preliminary analysis is run, in which a negative pressure of 0.01 MPa is applied to its inner surface of the inflated configuration, see figure 2 (top). Once deflated, the folded balloon can be inserted inside the stent, as shown in figure 2 (bottom). The expansion process of the stent-balloon system is reported in the pressure vs. diameter diagram of figure 3. We notice that, once the balloon has reached its nominal diameter, further increases in pressure have no significant effect on its size. This finding is consistent with the hypothesis of the semi-compliant balloon used in the reality, as shown by the comparison of the numerical results with the data supplied by the manufacturer reported in figure 3.

The coronary artery is modelled with an internal radius of 1.25 mm, a thickness of 0.5 mm and a length of 10 mm. The artery is meshed with 87750 8-node cubic solid elements. The material parameters used for the strain energy function, see equation 1, are defined referring to the mean values of experimental results in the circumferential direction obtained in [11] and are reported in table 1.

In order to verify the adequacy of the mesh density used in the simulations, a mesh dependency study expanding either the stent and artery to a diameter of 3 mm is performed. The unit stent mesh density is increased from 9969 to 19937 elements. The percentage difference of Von Mises stresses between the finest and selected meshes is of 0.3%. The artery mesh density is increased from 7050 to 280098 elements. No appreciable difference in Von Mises stresses between the finest and the selected meshes is observed.

The expansion of the balloon/stent device is computed following three main steps. First of all a pressure of 100 mmHg is imposed to the internal surface of the

artery to mimic the physiological conditions, see figure 4 (a). Then, the stent is expanded by applying a pressure of 1.5 MPa to the internal surface of the balloon. In particular, at a pressure p=0.135 MPa the balloon enters in contact with the stent, as shown in figure 4 (b). At a pressure p=0.285 MPa the balloon enters in contact with the artery showing the well-known dogboning-shape, see panel 4 (c). Increasing the pressure also the central part of the stent is expanded, as illustrated in panel 4 (d), up to the maximum expansion reached at p=1.5 MPa, corresponding to figure 4 (e). In this configuration the artery reaches a maximum internal diameter of 3.47 mm. Finally, the balloon is deflated, see figure 4 (f). The final artery lumen is of 3.06 mm. The deformed geometry of artery and stent obtained at the end of the simulation are stored to be used in the fluid dynamic analysis. Observing figure 4 (f) we notice that the parameters useful to quantify the interaction between the stent and artery and consequently the efficacy of drug elution may be:

1. the metal to artery ratio in the expanded configuration that measures the artery surface covered by the stent and hence of the area prone to a direct diffusion of the drug. In this case it is equal to 18%.

2. the foreshortening effect that is a measure of the contraction of the stent during the expansion and hence it gives an information about the length of the area interested by the drug release process..

3. the dogboning effect that quantifies the irregular expansion of the stent (grater in the external part than in the central one) and hence it is related with the irregularity of the artery internal surface that may influences the fluid dynamic phenomena.

In figure 5 are also reported radial, circumferential and axial Cauchy stress components: even if not directly used in the following analysis, they may be useful to better understand the effects of stent-balloon expansion on the artery configuration and eventually to highlight local conditions particularly unsafe.

Finally, we recall that refinements of the stent expansion geometrical and constitutive models will be useful for a more detailed and precise description of the process and hence for more precise initial conditions of blood flow and the drug deposition problem.

4.2 Analysis of the fluid dynamics around the struts

The lumen and the wall of the artery are subdivided with Gambit (ANSYS Inc., Canonsburg, PA, USA) into 1,637,336 and 1,118,420 tetrahedra respectively. In order to obtain an accurate resolution with a reasonable computational cost and memory storage, we have applied a nonuniform spacing for the mesh generation. In particular, the central part of the domain have been subdivided by means of variable size elements, particularly refined around the stent.

Looking at the Cordis BX-Velocity stent, it is possible to identify two kinds of structures, the struts and the links. The former are twisted rings that provide the circumferential strength of the stent, while the latter are tiny connections along the longitudinal axis between subsequent struts.

An important feature of the struts is to be twisted in the circumferential direction. For this reason, the blood flow hits the struts with different angles. The preliminary results obtained in [6] suggest that the flow pattern downstream the struts may be substantially different from the well-known flow after a backward facing step that corresponds to the ideal case of a perfectly circular ring that is orthogonal to the flow. This conjecture is confirmed by the fluid dynamics simulations. Indeed, in figure 6 we visualize the streamlines of the blood flow around the stent. This picture shows that we deal with a fully three dimensional flow with recirculations, vortexes and secondary motions. For instance, we observe that the vortex induced by the presence of the link on the top left corner is stretched and absorbed in the main stream on its right side. This suggests that this vortex is not only characterized by a planar rotating flow but an out of plane motion is present. This secondary motion generates the displacement of the fluid form the center of the vortex to the extrema and the fluid is thus cast out the vortex into the main stream.

In conclusion, there is evidence that the interaction between the stent and the blood stream generates very complex flow patterns where the recirculation zones downstream the obstacles interact with the main stream. By this way, the fluid that was at some time trapped into a recirculation may join the high speed flow. We will see in the next section that this behavior has important consequences on the drug release process.

4.3 Analysis of the drug release

As already mentioned, we simulate the release of heparin. According to the experimental investigations presented in [14], this corresponds to set $D_f = 1.5\ 10^{-4}$ mm^2/s, $D_w = 7.7\ 10^{-6}$ mm^2/s and $P = 4\ 10^{-4}$ mm/s. The diffusivity of the drug into the stent coating typically ranges from 10^{-8} to 10^{-12} mm^2/s, depending on the mechanical properties of the polymeric substrate. To avoid too stiff parameters we set $D_s = 10^{-8}$ mm^2/s.

The numerical simulation based on equation (3) shows that the drug released into the lumen is very quickly washed out by the blood flow. Indeed, the peaks of drug concentration into the lumen are reached about 40 seconds after the beginning of the process. This corresponds to only 1% of the time necessary to release almost all the drug form the stent. Conversely, the drug dynamics into the arterial walls is much slower, but after 1 hour the drug has reached the outer boundary of the arterial walls, as can be seen in figure 8 (bottom).

The drug concentration into the lumen is reported in figure 7. The highest peaks of drug concentration appear in the neighborhood of the links. In these regions, the contour plot of the concentration suggests that the recirculation of the blood flow interacts with the drug accumulation. The smooth and concave shape of the contours suggests that part of the drug released and accumulated in the neighborhood of the links is transported away and may affect the arterial walls located downstream. Indeed, regions related to non negligible concentration levels are clearly visible downstream the stent in figure 8 (top), where the presence of the drug in the lumen is visualized by means of the isosurface of the concentration. This means that a wide portion of the endothelium, which is often severely injured by the stent implantation, is exposedto a non negligible drug concentration. When the drug has anti-proliferative properties, the re-endothelialization process mey be slowed down. This seems to be one of the major drawbacks of DES, and it should be further investigated.

Concerning the struts, the accumulation of drug is unexpectedly prominent upstream with respect to the blood flow. High concentration levels take place where the struts are highly curved and their curvature is convex with respect to the blood flow. This is in contrast to the results obtained in [2], but can be explained observing that blood transports the drug downstream to the location where it has been released. The accumulation of the drug takes place where this effect is hindered by the convex stent pattern with respect to the blood flow.

The results reported in figure 7 (right) suggest that part of the drug released into

the lumen is absorbed by the wall. However, depending on the sign of the quantity $P(c_f - c_w)$ of equation (4), the opposite process is simultaneously happening, because the drug concentration in the wall is much higher than the one into the lumen in the surroundings of the interface of contact between the stent and the artery. Indeed, the interface Γ between the lumen and the walls can be subdivided into a region where the drug is absorbed into the wall and the complementary region where the drug is released by the wall and definitely lost into the blood flow.

This balance can be analyzed by means of more quantitative results. After 1 hour from the stent implantation, almost all the drug has been released. The contact interface between the stent and the walls ensures that 15% of the total amount of drug is released into the walls. However, more than a half of this fraction is simultaneously transferred into the lumen because of the negative concentration gradient between the lumen and the walls. Then, for the case analyzed here, the drug released into the lumen does not significantly contribute to the permanent drug deposition into the arterial wall. However, to come up to a general conclusion, further investigations are mandatory.

5 Conclusions

We have analyzed the interactions between the stent shape and positioning, the blood flow and the drug release from a stent, showing that a 3-dimensional analysis of the problem accounting for the complex geometry of the stent is mandatory to capture the phenomena into play. In this setting, we have studied the contribution of the drug released into the blood flow with respect to the efficacy of drug deposition and penetration into the arterial walls.

Acknowledgments

This work has been supported by the Italian Institute of Technology with the project "NanoBiotechnology - Models and Methods for Local Drug Delivery from Nano/Micro Structured Materials".

References

[1] F. Auricchio, M. Di Loreto, and E. Sacco. Finite-element analysis of a stenotic revascularization through a stent insertion. *Comput. Methods.*

Biomech. Biomed. Engin, 4:249–264, 2001.

[2] B. Balakrishnan, A.R. Tzafriri, P. Seifert, A. Groothuis, C. Rogers, and E.R. Edelman. Strut position, blood flow, and drug deposition. implications for single and overlapping drug-eluting stents. *Circulation*, 111:2958–2965, 2005.

[3] Erik Burman, Miguel A. Fernández, and Peter Hansbo. Continuous interior penalty finite element method for Oseen's equations. *SIAM J. Numer. Anal.*, 44(3):1248–1274 (electronic), 2006.

[4] Erik Burman and Peter Hansbo. Edge stabilization for Galerkin approximations of convection-diffusion-reaction problems. *Comput. Methods Appl. Mech. Engrg.*, 193(15-16):1437–1453, 2004.

[5] Erik Burman and Paolo Zunino. A domain decomposition method based on weighted interior penalties for advection-diffusion-reaction problems. *SIAM J. Numer. Anal.*, 44(4):1612–1638 (electronic), 2006.

[6] Carlo D'Angelo and Paolo Zunino. A numerical study of the interaction of blood flow and drug release from cardiovascular stents. Proceedings of the Enumath Conference, Austria, September 2007, MOX, Department of Mathematics, Politecnico di Milano, 2007. Submitted.

[7] C.T. Gasser and G.A. Holzapfel. Finite element modeling of balloon angioplasty by considering overstretch of remnant non-diseased tissues in lesions. *Comput. Mech.*, 40:47–60, 2007.

[8] F. Gervaso, C. Capelli, L. Petrini, S. Lattanzio, L. Di Virgilio, and F. Migliavacca. On the effects of different strategies in modelling balloon-expandable stenting by means of finite element method. *J. Biomech.*, 2007. Submitted.

[9] T. Higuchi. Rate of release of medicaments from ointment bases containing drugs in suspension. *J. Pharmac. Sci.*, 50:874–875, 1961.

[10] G.A. Holzapfel. *Encyclopedia Of Computational Mechanics*, pages 605–635. John Wiley & Sons, Ltd, Chichester, 2004. Edited by Erwin Stein, René de Borst and Thomas J.R. Hughes.

[11] G.A. Holzapfel, G. Sommer, C.T. Gasser, and P. Regitnig. Determination of layer-specific mechanical properties of human coronary arteries

with nonatherosclerotic intimal thickening and related constitutive modelling. *American Journal of Physiology, Heart and Circulatory Physiology*, 289:2048–58, 2005.

[12] D.R. Hose, A.J. Narracott, B. Griffiths, S. Mahmood, J. Gunn, D. Sweeney, and P.V. Lawford. A thermal analogy for modelling drug elution from cardiovascular stents. *Comput. Methods. Biomech. Biomed. Engin*, 7:257–264, 2004.

[13] G. Karner and K. Perktold. Effect of endothelial injury and increased blood pressure on albumin accumulation in the arterial wall: a numerical study. *J. Biomech.*, 33:709–715, 2000.

[14] M.A. Lovich and E.R. Edelman. Mechanisms of transmural heparin transport in the rat abdominal aorta after local vascular delivery. *Circ. Res.*, 77:1143–1150, 1995.

[15] F. Migliavacca, F. Gervaso, M. Prosi, P. Zunino, S. Minisini, L. Formaggia, and G. Dubini. Expansion and drug elution model of a coronary stent. *Comput. Methods. Biomech. Biomed. Engin*, 10:63–73, 2007.

[16] F. Migliavacca, L. Petrini, M. Colombo, F. Auricchio, and R. Pietrabissa. Mechanical behavior of coronary stents investigated by the finite element method. *J. Biomech.*, 35:803–811, 2002.

[17] M. Prosi, P. Zunino, K. Perktold, and A. Quarteroni. Mathematical and numerical models for transfer of low-density lipoproteins through the arterial walls: a new methodology for the model set up with applications to the study of disturbed lumenal flow. *J. Biomech.*, 38:903–917, 2005.

[18] Alfio Quarteroni and Alberto Valli. *Domain decomposition methods for partial differential equations*. Numerical Mathematics and Scientific Computation. The Clarendon Press Oxford University Press, New York, 1999. Oxford Science Publications.

[19] Alfio Quarteroni, Alessandro Veneziani, and Paolo Zunino. Mathematical and numerical modeling of solute dynamics in blood flow and arterial walls. *SIAM J. Numer. Anal.*, 39(5):1488–1511 (electronic), 2001/02.

[20] G. Rappitsch and K. Perktold. Pulsatile albumin transport in large arteries: a numerical simulation study. *J. Biomech. Eng.*, 118:511–519, 1996.

[21] G. Rappitsch, K. Perktold, and E. Pernkopf. Numerical modelling of shear-dependent mass transfer in large arterie. *Int. J. Numer. Meth. Fluid*, 25:847–857, 1997.

[22] D.V. Sakharov, L.V. Kalachev, and D.C. Rijken. Numerical simulation of local pharmacokinetics of a drug after intravascular delivery with an eluting stent. *J. Drug Targ.*, 10(6):507–513, 2002.

[23] D.K. Stangeby and C.R. Ethier. Computational analysis of coupled blood-wall arterial ldl transport. *J. Biomech. Eng.*, 124:1–8, 2002.

[24] A.R. Tzafriri and E.R. Edelman. On the validity of the quasi-steady state approximation of bimolecular reactions in solution. *J. Theor. Biol.*, 233:343–350, 2005.

[25] Christian Vergara and Paolo Zunino. Multiscale modeling and simulation of drug release from cardiovascular stents. Technical Report 15, MOX, Department of Mathematics, Politecnico di Milano, 2007. Submitted.

[26] N.L. Wang and K.H. Keller. Augmented transport of extracellular solutes in concentrated erytrocyte suspensions in couette flow. *J. Colloid Inter. Sci.*, 103:210–225, 1985.

Figures

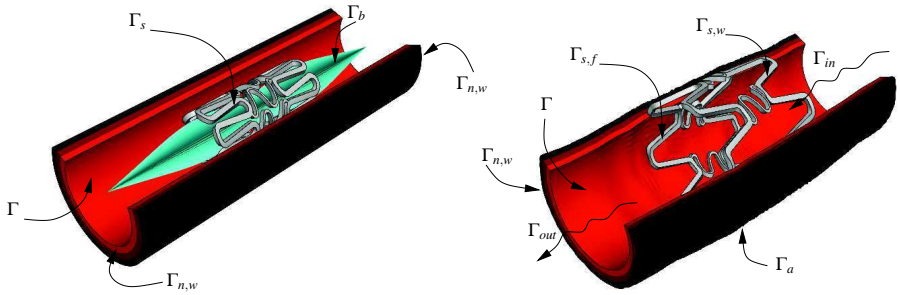

Figure 1: The lumen and the arterial wall with the partition of their boundaries for the set up of the mechanical model of the expansion of the stent (left) and of the drug release after the expansion (right).

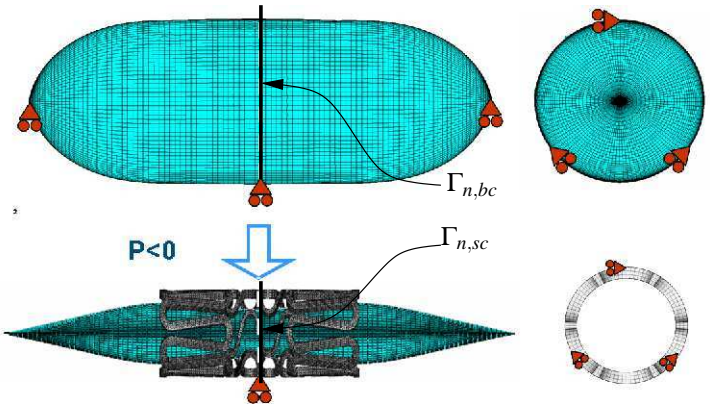

Figure 2: Boundary conditions and computational mesh of the balloon-stent model.

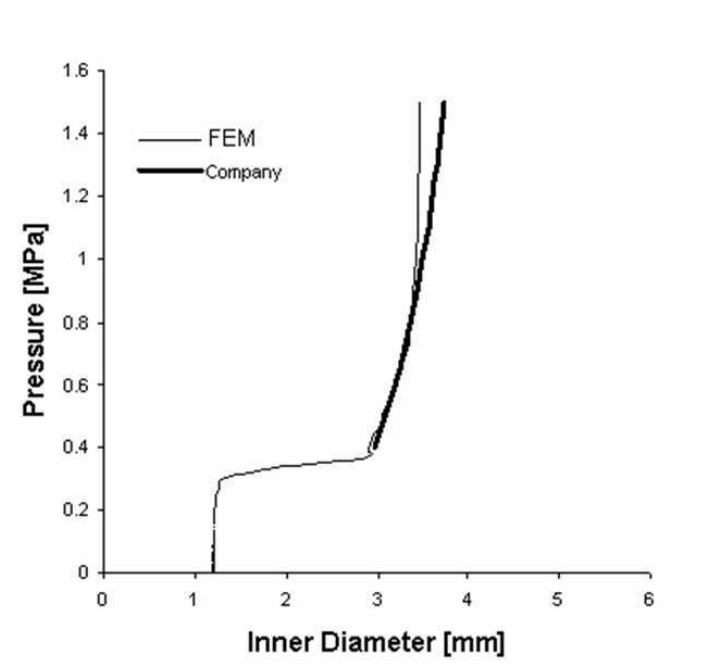

Figure 3: Pressure-diameter curve of the balloon-stent model compared to the data available from the manufacturer

.

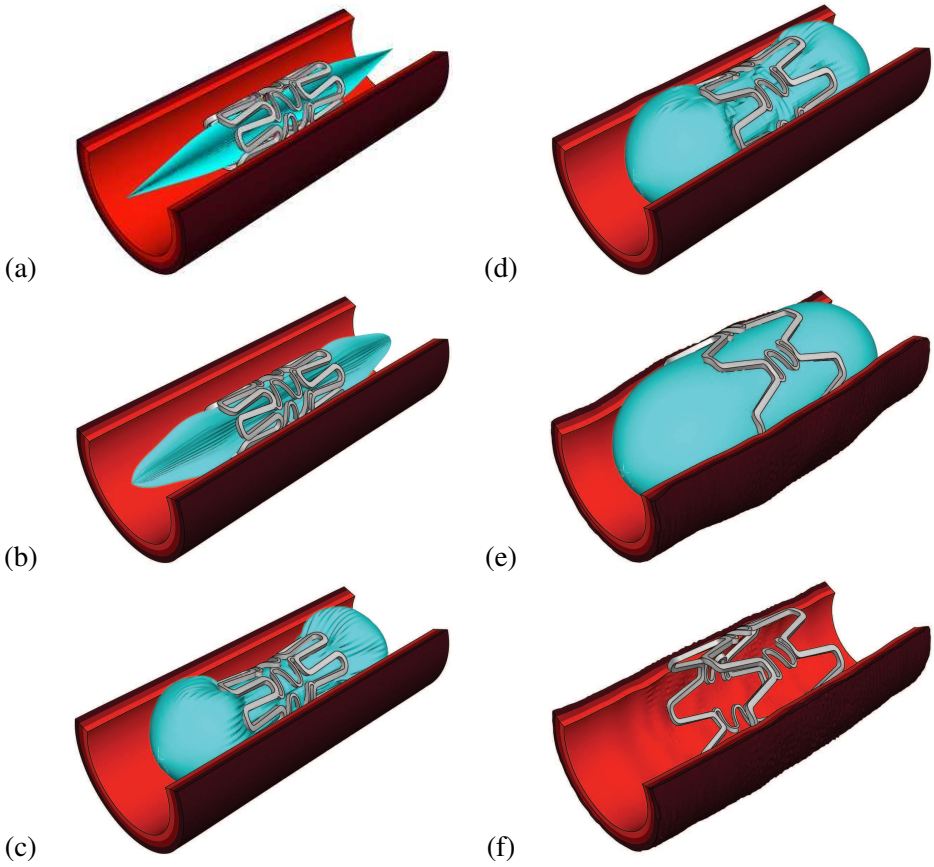

Figure 4: The sequence of steps describing the expansion of the stent.

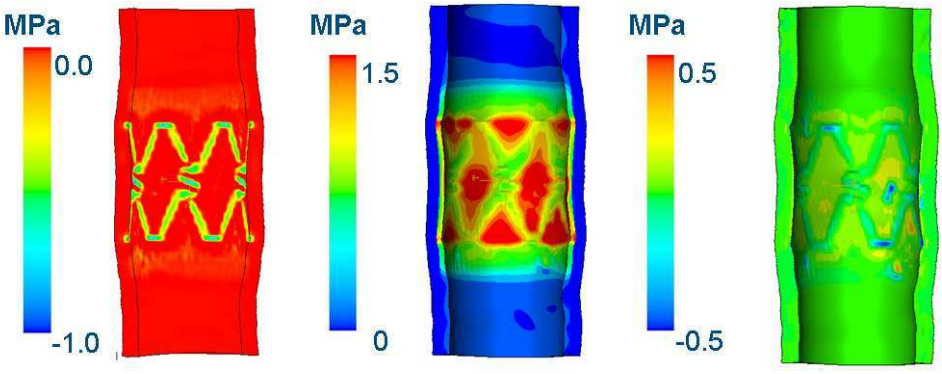

Figure 5: Radial, circumferential and axial Cauchy stresses on the artery.

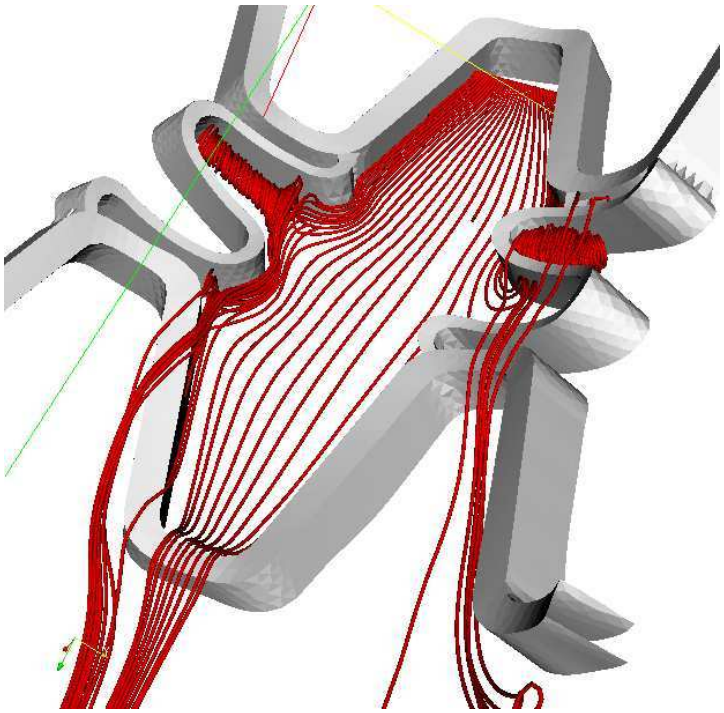

Figure 6: The interaction between the stent and the blood flow visualized by means of streamlines. The proximal section is located on the top while the distal section in on the bottom.

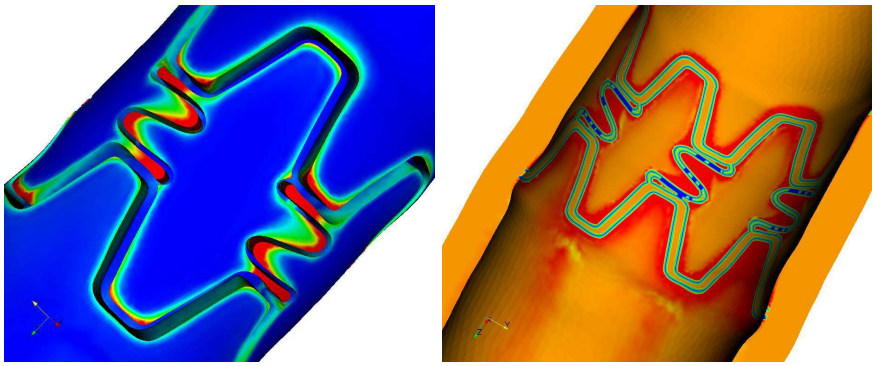

Figure 7: The contour plots of the concentration in the arterial lumen at 40 seconds after the beginning of the process are shown on the bottom/left, the color scale ranges linearly from 0 (blue) to $10^{-3}c_s^0$ (red). The mass flux exchanged between the lumen and the arterial wall is on the bottom/right. The red color denotes a positive flux from the lumen to the wall, the blue color refer to the opposite case.

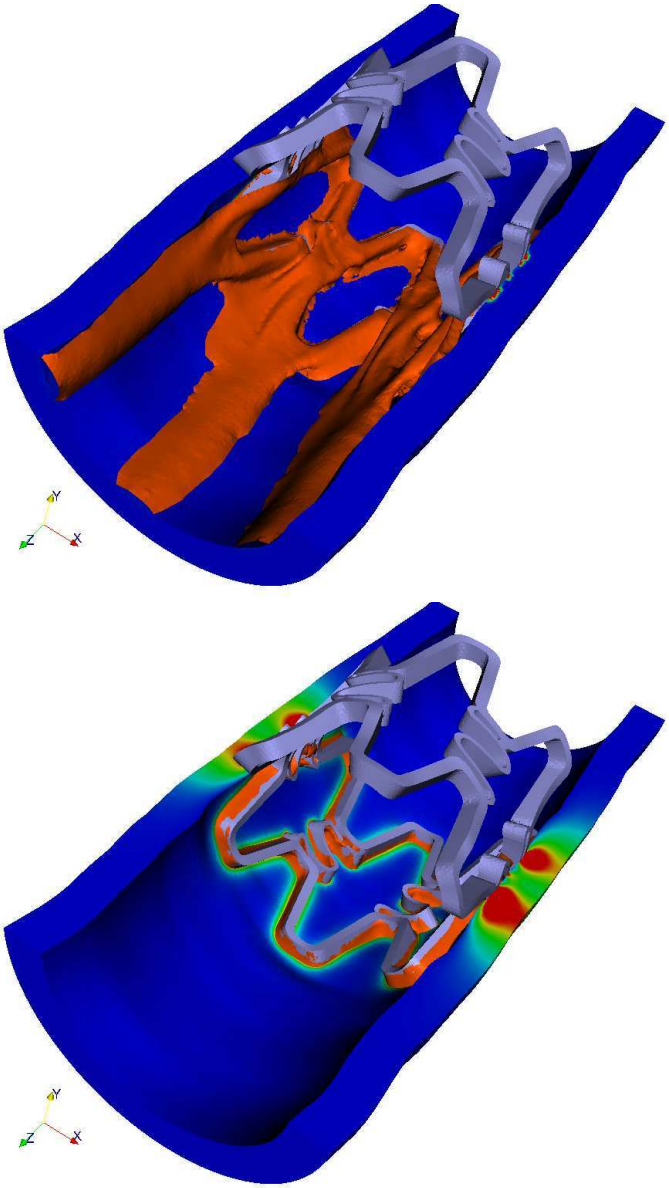

Figure 8: The isosurface corresponding to the value $10^{-5}c_s^0$ for the drug concentration in the arterial lumen and contour plots into the arterial walls, at 40 seconds (top) and 1 hour (bottom) after the beginning of the process. The color scale ranges linearly form 0 (blue) to $10^{-3}c_s^0$

Tables

	C_{10}	C_{20}	C_{30}	C_{40}	C_{50}	C_{60}
Intima	6.79E-03	0.54	-1.11	10.65	-7.27	1.63
Media	6.52E-03	4.89E-02	9.26E-03	0.76	-0.43	8.69E-02
Adventitia	8.27E-03	1.20E-02	0.52	-5.63	21.44	0.00

Table 1: Coronary artery model parameters.